Exciton Broadening in WS_2/Graphene Heterostructures

Heather M. Hill[1,2], Albert F. Rigosi[1,2], Archana Raja[1,2], Alexey Chernikov[1,3], Cyrielle Roquelet[1,4], and Tony F. Heinz[1,2]

[1]*Departments of Physics, Electrical Engineering, and Chemistry, Columbia University, New York, NY 10027, United States*

[2]*Department of Applied Physics, Stanford University, Stanford, CA 94305, United States; and SLAC National Accelerator Laboratory, 2575 Sand Hill Road, Menlo Park, CA 94025, United States*

[3]*Department of Physics, University of Regensburg, Regensburg 93053, Germany*

[4]*ArcelorMittal Maizières Research SA, Maizières-lès-Metz 57280, France*

ABSTRACT: We have used optical spectroscopy to observe spectral broadening of WS_2 exciton peaks in heterostructures of monolayer WS_2 capped with mono- to few-layer graphene. The broadening is found to be similar for the A and B excitons and on the order of 5 to 10 meV. No strong dependence on the number of graphene layers was observed within experimental uncertainty. The broadening can be attributed to charge and energy transfer processes between the two materials, providing an observed lower bound for the corresponding timescales of 65 fs.

I. INTRODUCTION

Due to its unique electronic and optical properties [1-4], graphene is a promising material for use in optoelectronics and photovoltaics. The extensive study of graphene has led to the investigation of the semiconducting transition-metal dichalcogenide semiconductors (TMDCs),

which exhibit direct gaps as monolayers [5-9], strong light emission and absorption in the visible range [10-15], coupled valley and spin degrees of freedom [16-25], and large exciton and trion binding energies [26-35]. Combinations of TMDC layers and graphene have already been assembled into heterostructures [36], photodetectors [37], multifunctional photoresponsive memory devices [38], and vertical field effect transistors [39]. Much recent effort has been focused on interlayer interactions in TMDC heterostructures [40-52]. Specifically, charge transfer processes have been invoked to explain line broadening observed in the excitonic features in TMDC/TMDC heterostructures compared to the corresponding linewidth in the isolated monolayers [51]. The broadening effects, as well as narrowing effects that may arise from reduced static charging and the screening of inhomogeneous potentials from the substrate, as seen in TMDC/hexagonal boron nitride (h-BN) heterostructures [53], are expected to play a role in the case of TMDC/graphene heterostructures. Such TMDC/graphene structures have been introduced for various device applications and have also been of particular interest in the spectroscopy community [54-57]. In a recent report, we examined the influence of graphene on renormalization of the TMDC bandgap due to dielectric screening in graphene-covered TMDC samples [58], determined spectroscopically through characterization of the fundamental Rydberg exciton series.

In this paper, we examine changes in the linewidth of excitons in the TMDC monolayers caused by the presence of an adjoining graphene layer in a vertical heterostructure. Through careful absorption measurements of the A and B excitons in monolayer WS_2, we identify exciton line broadening of at least 5 meV induced by mono- and few-layer graphene. We discuss the possible mechanisms responsible for this observation, particularly the impact of the fundamental processes of energy and charge transfer from the semiconducting WS_2 to graphene. Our study

provides an upper bound on the observed rate of these processes and, hence, a lower limit for the energy and charge transfer times extracted from the observed broadening. These results also complement the recent time-resolved pump-probe studies of TMDC/graphene heterostructures [59].

II. EXPERIMENTAL METHODS

A. Sample Preparation

The monolayer WS_2 samples were prepared by exfoliating bulk crystal onto fused silica substrates. We verified the layer thickness using photoluminescence (PL) and Raman spectroscopy. Subsequently, graphene was exfoliated on polypropylene carbonate (PPC) that was spin-cast on a silicon wafer. The thickness of the exfoliated graphene was confirmed with Raman spectroscopy and reflectance contrast measurements. We found mono-, bi-, tri-, and tetra-layer graphene flakes. The selected graphene layers were then transferred onto monolayer WS_2 flakes following the procedure described in the Supplemental Material of Ref. 51. The residual PPC was removed with acetone followed by an isopropanol rinse. The samples were not annealed to prevent any modification to their optical properties. To facilitate spectroscopic comparison, the structure was prepared so that there were accessible regions of uncovered, pristine WS_2 in addition to the WS_2/graphene heterostructure.

B. Reflectance Contrast Measurements

We obtained information about the optical absorption of the sample by measuring the reflectance spectrum from the sample on the substrate, Rs, as well the corresponding spectrum for the bare substrate, R_0. We then constructed the reflectance contrast spectrum as $\Delta R/R = (Rs - R_0)/R_0$. For a thin sample with low absorption on a transparent substrate, as in our measurements,

this reflectance contrast spectrum is proportional to the absorption of the sample [6]. The reflectance measurements were performed using a tungsten-halogen lamp light source focused on the sample at normal incidence with a spot size of 2 μm. The reflected light was collected by a spectrometer equipped with a CCD cooled by liquid nitrogen (LN). Our measurements were mostly conducted with samples at room temperature, and some samples were cooled in a cryostat to 70 K with LN. Measurements showing the extent of PL quenching and its relation to the observed exciton line broadening are provided in section 5 of the Supplemental Material [60].

For each of the samples, the reflectance contrast spectrum was measured in three different regions: on bare WS_2 without graphene above it (both before and after heterostructure processing), on graphene on fused silica without WS_2 below it, and on the graphene/WS_2 heterostructure. The variation in exciton linewidth determined at several different points on the WS_2 samples was found to be less than 0.5 meV. This result indicates that the inhomogeneity of the sample was minor. We also determined that the linewidth of the WS_2 exciton in the isolated region of the material did not change more than 0.5 meV during the processing (*i.e*., mechanical transfer) required to prepare the heterostructure. See section 7 of the Supplemental Material for more details [60].
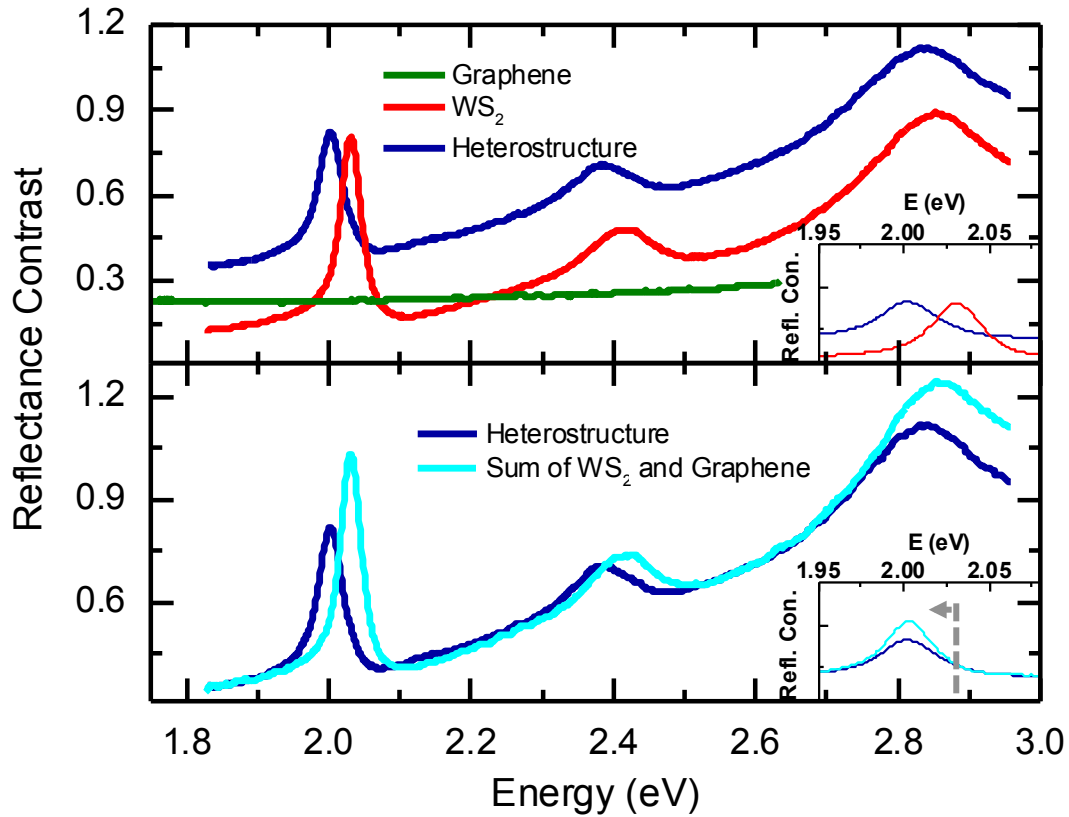
III. EXPERIMENTAL RESULTS

FIG. 1. (Color online) (**Top**) The room-temperature reflectance contrast spectrum of 1L WS_2, 2L graphene, and WS_2/graphene heterostructure are shown. The red curve is the reflectance contrast of WS_2 on fused silica without graphene and the green line is the reflectance contrast of bilayer graphene on fused silica. The dark blue is the WS_2/graphene heterostructure. The inset presents an expanded view in of the A exciton. (**Bottom**) A comparison is made between the reflectance contrast of the heterostructure and the sum of the spectra of the constituent layers. The blue curve is the experimental reflectance contrast data from the heterostructure (as in the top half of the Figure). The cyan curve is obtained by adding the graphene reflectance contrast spectrum to

that for a bare WS_2 monolayer. The inset shows the A exciton features for both curves, with the summed curve redshifted by 23 meV to allow for a direct comparison of the lineshapes.

Figure 1 shows reflection contrast spectra for the case of a heterostructure composed of monolayer WS_2 and bilayer graphene, as measured at room temperature. For the heterostructure, an expected increase in the reflection contrast occurs due to the broad absorption of graphene. However, the heterostructure spectrum is not simply the sum of the isolated WS_2 and graphene absorption spectra. To demonstrate this, we plot in the bottom half of Figure 1, the summed graphene and WS_2 spectrum compared to the measured heterostructure spectrum. We note two major differences: the measured exciton peaks in the heterostructure are broadened and redshifted. The bottom inset of Figure 1 includes a redshifted, summed spectrum to allow a more direct comparison of the width of the A exciton peaks. We attribute the redshift is screening by dielectric environment associated with the graphene. The relatively modest observed shift in the exciton transition energy reflects the combination of a significant renormalization of the quasiparticle bandgap, offset by a decrease in the exciton binding energy [58].
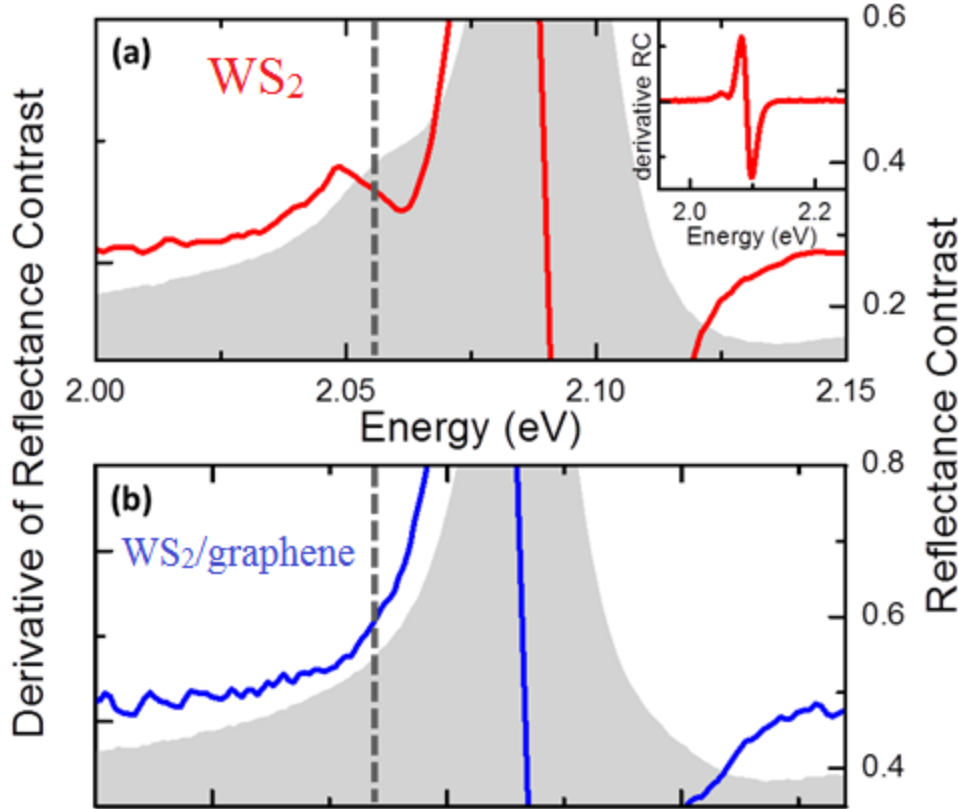
FIG. 2. (Color online) Trion feature of the A exciton in the reflectance contrast spectrum of bare WS$_2$ and of the WS$_2$/graphene heterostructure, as measured at 70 K. (a) For bare WS$_2$, the (energy) derivative of the reflectance contrast spectrum is shown as a blue line. The grey shading (right vertical scale) is the reflection contrast spectrum itself. The derivative of the reflectance contrast is plotted over a larger energy range in the inset. The position of the trion is indicated by a vertical dashed line. (b) The same data is plotted for a WS$_2$/graphene heterostructure. In this case, there is no signature of the trion absorption.

In Figure 2, we present reflectance contrast spectra for the sample at a temperature of approximately 70 K. In each panel, we also show the spectrum's derivative, with respect to energy, to bring out weak features. As is typical for exfoliated samples on a substrate [27], a trion feature appears in the reflectance contrast of bare WS$_2$ due to unintentional doping of the sample. The corresponding peak position is about 2.05 eV, on the low-energy shoulder of the

neutral A exciton. When WS_2 is capped with graphene, as shown in Figure 2(b), the trion feature disappears. The absence of a trion feature for the WS_2/graphene heterostructure is not unexpected, since residual charges in the WS_2 could flow into lower-energy states via *static* charge transfer in the semi-metallic graphene layer, whose Fermi energy is located in the gap of the WS_2. The evidence of *static* charge transfer to graphene, coupled with Raman spectroscopy data provided in section 6 of the Supplemental Material [60], will assist us in our overall interpretation of the exciton broadening in the discussion section.

   To analyze the exciton line broadening more precisely, we can simulate the experimental data by starting with summed and redshifted WS_2 and graphene spectra for the isolated layers and then convolving this spectrum for non-interacting layers with a Lorentzian line shape. The width of the Lorenztian is separately optimized for the A and B exciton features. Alternatively, we can simply fit exciton features in the isolated WS_2 to a Lorenztian line and compare this width to that obtained in a similar fashion for the heterostructure. The latter procedure gives a broadening several meV less than the former, but assumes negligible inhomogeneous broadening in the fitting process. The convolution method does not require any particular assumptions with respect to the underlying peak structure and lineshape, since the spectra include both minor features from excited exciton states, as well as the broad shoulder from higher energy resonances, such as the C-feature.
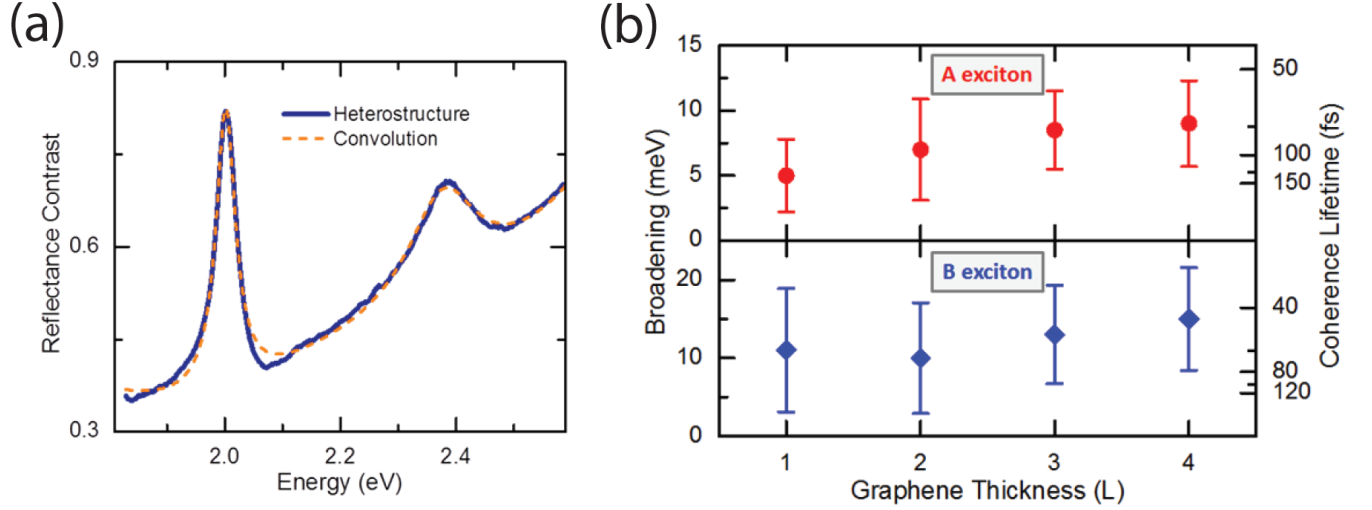
FIG. 3. (Color online) (a) Room temperature reflectance contrast of a heterostructure is shown as well as the convolution of the sum of the individually measured constituent layers' spectra with a Lorentzian profile. The blue curve is the experimental reflectance contrast data from the heterostructure shown in Figure 1. The dashed orange curve comes from convoluting the sum of the graphene and bare WS_2 reflectance contrast with a Lorentzian profile of 7 meV. (b) Linewidth broadening and coherence lifetimes for the A and B exciton of WS_2 in the heterostructure are presented as a function of the thickness of the graphene; the data were taken at room temperature. The top and bottom halves of the graph show the broadening of the A and B exciton peaks in the reflectance contrast, respectively. The thickness of the graphene is given in terms of layer numbers (L). Coherence lifetimes are obtained from the relation $\tau = \hbar/\Delta\Gamma$, accompanied by error bars associated with the extracted broadening uncertainty. The experimental range of lifetimes extracted with convolutions is 65 fs – 130 fs, compared with the 55 fs – 100 fs lifetime range extracted with the individual Lorentzian peak fitting, which assumes an ideal system and thus provides an even lower, yet theoretical, bound to the lifetimes.

In Figure 3(a), we compare the experimental reflectance contrast spectrum of the A exciton of the heterostructure with the reflectance contrast spectrum for non-interacting layers (*i.e.* taking the sum of the measured spectra of bare WS_2 and bare graphene). The latter spectrum was then convoluted with a Lorentzian peak to simulate the broadening we observe in the heterostructure's experimental data. The Lorentzian width, given by $\Delta\Gamma$, in the convolution

integral provides an upper bound for the observed increase in homogeneous linewidth. If this broadening arises from a new decay channel for WS_2 excitons due to the presence of graphene, we then have a lower bound for the observed lifetime of this process, given by $\tau = \hbar/\Delta\Gamma$.

The broadening values and associated lifetimes for the A and B exciton transitions are shown in Figure 3(b) as a function of the thickness of the graphene that is placed on top of the WS_2. We see that, within experimental uncertainty, the broadening does not have a strong dependence on graphene thickness up to tetra-layer graphene and ranges between 5 and 10 meV. Overall, the broadening is 4 to 5 times less than that seen in TMDC/TMDC heterostructures [42,51,61], which was attributed to interlayer (i.e. not *static*) charge transfer.

IV. DISCUSSION

A. Phonon Broadening and Doping

We now discuss possible physical mechanisms leading to the exciton line broadening in the WS_2/graphene heterostructure. Several possible mechanisms can be identified, including: enhanced phonon broadening in the heterostructure, changes in doping, intervalley scattering within or between layers, i.e., including charge transfer, as well as energy transfer processes. The mention of charge transfer in the following arguments is *not* a reference to the distinct *static* charges moving from WS_2 to graphene upon the layers making initial contact. We proceed to argue that the dominant processes to consider are indeed the latter two phenomena: energy and charge transfer of photoexcited carriers from WS_2 to graphene.

At room temperature, the A exciton peak in a typical exfoliated monolayer WS_2 A peak has a width of about 40 ($\pm$10) meV, as is also the case in our samples. As indicated by temperature-resolved measurements and theoretical modelling [62,63], about 20 meV of this linewidth

primarily arises from exciton scattering with thermally activated phonons and a small contribution from the radiative recombination on the order of several meV. When the WS_2 flake is in contact with graphene, we could in principle expect to see increased phonon scattering from interaction of excitons in WS_2 with the phonons in the graphene layer. However, this additional scattering is unlikely given the expected inefficiency of such a process due to the small extension of the exciton wavefunction into the out-of-plane direction. That is further supported by the observation of similar increases in the exciton linewidth at low temperatures, where the exciton-phonon-scattering contribution already in the WS_2 layer is on the order of only a few meV [63]. While the width of the excitonic features change quite dramatically (the 70 K temperature spectrum is available in the Supplemental Material [60]), the broadening does not change to within 1 meV. This also implies that the processes giving rise to the broadening does not strongly depend on the temperature, unlike what we would expect for an additional exciton-phonon scattering channel.

As previously discussed in Figure 2, the trion feature, seen clearly in the low energy shoulder of the A exciton in the WS_2 spectrum, has undergone a strong reduction in the heterostructure spectrum. The bare WS_2 spectrum indicates doping on the order of 3×10^{12} cm^{-2}, as extracted from the trion-exciton separation energy [64], typical for exfoliated samples on substrates. The heterostructure spectrum, however, has no obvious trion feature, strongly suggesting that the doping conditions across the WS_2 sample in contact with graphene are close to charge neutrality due to the expected transfer of the *static* charge to graphene. A change in the initial doping of a sample can change the width of the excitonic features in the reflectance contrast. However, typically a reduction in the doping would cause the peaks to become narrower, as previously observed in WS_2 monolayers [64]. In this case, a de-doping of a maximum carrier density of

3×10^{12} cm^{-2} would correspond to a linewidth narrowing of about 3 meV in contrast to the observed increase of the linewidth [64]. Therefore, the change in doping cannot be considered as the cause of the observed broadening and may even lead to an overall underestimation of the extracted values for the broadening by a few meV.

B. Intervalley Scattering as a Source of Broadening

In our system, the arbitrary angle between the layers and the general reconfiguration of the WS$_2$ band structure in the heterostructure may introduce intervalley scattering within the WS$_2$ layer as another possible broadening mechanism, which comes from two potential sources. The first source would be from the possibility that the band structure of WS$_2$ reconfigures such that it exhibits an indirect bandgap at the Q or Γ point. The second source would be from the potential overlap or hybridization of electronic states from WS$_2$ with those in graphene at various parts of the Brillouin zone (BZ), perhaps at the K point in the case of resonant tunneling.

In the first case, one should consider that the difference between the valence band energy of Γ and K in the unperturbed, direct gap case, is 0.1 eV for monolayer MoS$_2$, suggesting a 0.3 eV maximum shift due to the presence of graphene [65]. In the case of WS$_2$/graphene heterostructures, we consider that the Γ point maximum is 0.3 eV below that of the K point in the case using angle-resolved photoemission spectroscopy (ARPES) [66]. MoS$_2$/graphene heterostructures have been reported to form indirect occur at the Γ point (with a difference less than 0.2 eV with the K point) [36], but other literature suggests that MoS$_2$/graphene retains its direct band gap [66]. Therefore, if the graphene layer causes a similar change in the WS$_2$, it is unlikely that WS$_2$ forms an indirect bandgap. In the second case, ARPES measurements suggest that there is no significant overlap of electronic states at the K, Q, or Γ point between graphene and WS$_2$ [66,68]. We will revisit this second case in the charge transfer discussion.

The remaining two significant processes to consider are charge and energy transfer.

The fastest timescales for either charge transfer or energy transfer to occur in this system is on the order of 100 fs, as extracted from the experimental linewidth broadening. If we compare our system to other low-dimensional systems, we can approximate the contribution from non-radiative energy transfer via near-field dipole-dipole interactions. As an example, the energy transfer rate from nanoparticles and nanoplatelets to graphene has been reported to be around 1 ns, where the distance from the emitter to graphene is on the order of a few nanometers [69-71]. Federspiel et al. experimentally observed a d^{-3} dependence for the energy transfer rate between 2D CdSe nanoplatelets and graphene [72]. Hernández-Martínez et al. calculate a d^{-4} energy transfer rate between general 2D-2D interfaces [73], though at short length scales, the scaling deviates from this form when taking into account the non-local effects for graphene that become prominent at distances below 1 nm [57,73]. Gaudreau et al. also predict a similar enhancement in rates as a function of the distance to graphene [74]. We use both of these distance dependences to obtain a range of expected energy transfer rates. The separation between the donor and acceptor in our system is 0.5 nm from AFM measurements (see Supplemental Material [60]). If we scale the 1 ns rate mentioned above, we obtain an expected rate for our system of 3 ps to 0.2 ps or a broadening of 0.2 meV to 2 meV. And furthermore, the enhanced oscillator strength for WS_2 in Ref. 27 compared to the platelets should further increase the rate of energy transfer and broadening of the exciton line [75]. It is therefore conceivable that energy transfer contributes to the observed exciton broadening.

Concerning charge transfer, reported rates fall into a similar range for rare-gas adlayers on metal surfaces and similar systems (10-100 fs) [76-77]. Recent literature reports charge transfer rates of tens of femtoseconds in TMDC/TMDC heterostructures [51,62]. Based on the previous

discussion about treating the WS_2/graphene heterostructures as having a direct bandgap, one must question whether charge can transfer from the K point of WS_2 into graphene directly or via phonon-assisted process, which is set to occur as low of phonon energies as 84 meV, based on the alignment parameters in Reference 59. To elaborate, since the basic reciprocal lattice parameters in WS_2 and graphene are 1.33 Å^{-1} and 1.69 Å^{-1}, respectively, 0.36 Å^{-1} is the absolute momentum difference between the two K points only in the case where both materials are aligned. In this zero-degree orientation, one can depict the two materials' dispersions, as in Figure 4, to see that a phonon is required to impart at least 0.36 Å^{-1} of additional momentum, which is equivalent to 84 meV when the effective mass of the charge is $0.16m_0$ [27], to transfer charge from WS_2 to graphene. Since various Raman modes exist in WS_2, such as the $E^1_{2g}(\Gamma)$ and $A_{1g}(\Gamma)$, with respective energies of approximately 44 and 52 meV and corresponding to 355 cm^{-1} and 417 cm^{-1} [78], along with the consideration that excitons have an approximate radius in k-space of about 0.15 Å^{-1} [27], it is reasonable to expect that the various modes of WS_2 can contribute to charge transfer in these systems. Further analysis on the Raman and PL spectra corresponding to changes in the dielectric environment and reflectance is included in the Supplemental Material [60, 79-84].
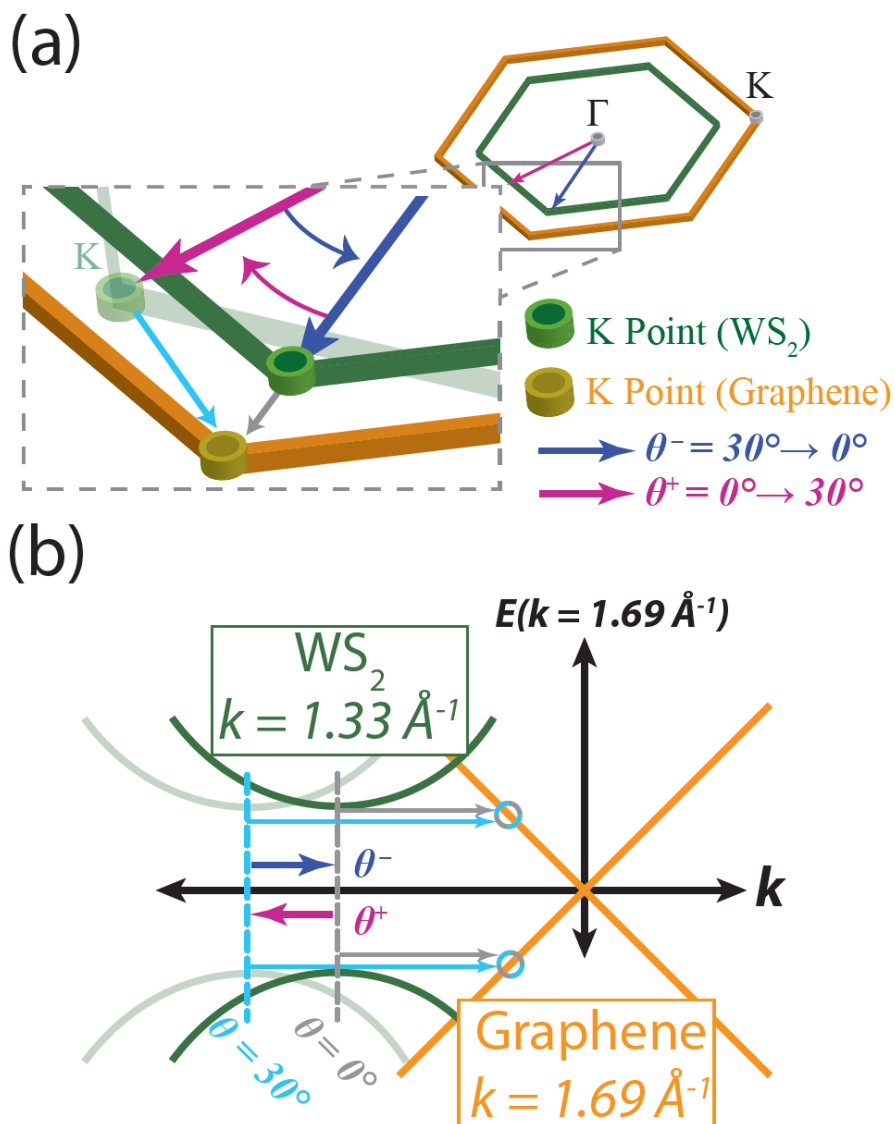
FIG. 4. (Color online) A schematic is shown to elucidate the reason why resonant charge transfer is very unlikely as well as the concept of non-resonant charge transfer, a phenomenon likely to occur in the WS$_2$/graphene heterostructure. (a) The Brillouin zones of graphene (in orange) and WS$_2$ (in dark green) are depicted along with the K points in each. One corner of the zone is inspected more closely, showing that the relative orientation of the two zones can vary depending on the crystal orientations (which were arbitrary when the mechanical transfers were performed). The dark blue and magenta arrows from the Γ point to the K point of WS$_2$ indicate a 0° and 30° crystal orientation, respectively. The light gray and cyan arrows from the K point of

WS_2 to the K point of graphene illustrate phonon-assisted charge transfer possibilities. (b) A graphical interpretation of the basic band structures of WS_2 and graphene shows that as one rotates the WS_2 Brillouin zone from 0° to 30° (magenta angular arc in (a)), the relative momentum difference between the K points of the two materials increases, represented by the color cyan. When the rotation is reversed, the K points of the two materials return to a relative momentum difference minimum, shown as a light gray dotted line and a corresponding light gray arrow signifying the necessity for phonon-assistance should charge transfer occur.

Recent pump-probe measurements of the WS_2/graphene system provide an upper bound for the charge transfer process, as determined by the experimental time resolution, of 350 fs [59]. Based on ARPES measurements, and assuming that both materials' Brillouin zones are at a zero-degree orientation with respect to each other, approximately 1.4 and 0.9 eV is required for the electron and hole, respectively, to initiate a charge transfer process without phonon assistance [59]. When comparing our results to the bounds determined by other experimental methods, we find that they agree, thereby adding support to the conclusion that charge transfer processes contribute to the observed exciton broadening.

V. CONCLUSIONS

In conclusion, by analyzing the reflectance contrast of bare WS_2 with that of various WS_2/graphene heterostructures, we are able to identify a 5 to 10 meV broadening in the exciton transitions of WS_2 induced by the presence of graphene. Both charge transfer and energy transfer were identified as the primary phenomena contributing towards this broadening. Within experimental uncertainty, the broadening was found to have negligible dependence on the graphene thickness. The extracted values of 65 fs to 130 fs are a lower bound of the timescales of both energy and charge transfer processes.

ACKNOWLEDGMENTS

REFERENCES

[1] K. S. Novoselov, A. K. Geim, S. V. Morozov, D. Jiang, Y. Zhang, S. V. Dubonos, I. V. Grigorieva, and A. A. Firsov, Science **306**, 666–669, (2004).

[2] A. K. Geim and K. S. Novoselov, Nat. Mater. **6**, 183–191, (2007).

[3] A. K. Geim, Science **324**, 1530–1534, (2009).

[4] M. Bernardi, M. Palummo, and J. C. Grossman, Nano Lett. **13**, 3664– 3670 (2013).

[5] K. S. Novoselov, D. Jiang, F. Schedin, T. J. Booth, V. V. Khotkevich, S. V. Morozov, and A. K. Geim, Proc. Natl. Acad. Sci. U.S.A. **102**, 10451 (2005).

[6] K. F. Mak, C. Lee, J. Hone, J. Shan, and T. F. Heinz, Phys. Rev. Lett. **105**, 136805 (2010).

[7] A. Splendiani, L. Sun, Y. Zhang, T. Li, J. Kim, C. Chim, G. Galli, and F. Wang, Nano Lett. **10**, 1271– 5 (2010).

[8] W. Zhao, Z. Ghorannevis, L. Chu, M. Toh, C. Kloc, P. Tan, and G. Eda, ACS Nano **7**, 791– 797 (2013).

[9] C. Ruppert, O. B. Aslan, and T. F. Heinz, Nano Lett. **14**, 6231 (2014).

[10] G. Eda, H. Yamaguchi, D. Voiry, T. Fujita, M. Chen, and M. Chhowalla, Nano Lett. **11**, 5111– 5116 (2011).

[11] L. Britnell, R. Ribeiro, A. Eckmann, R. Jalil, B. Belle, A. Mishchenko, Y.-J. Kim, R. Gorbachev, T. Georgiou, and S. Morozov, et al, Science **340**, 1311 (2013).

[12] C.-C. Shen, Y.-T. Hsu, L.-J. Li, and H.-L. Liu, Appl. Phys. Express **6**, 125801 (2013).

[13] Y. Li, A. Chernikov, X. Zhang, A. Rigosi, H. M. Hill, A. M. van der Zande, D. A. Chenet, E.-M. Shih, J. Hone, and T. F. Heinz, Phys. Rev. B **90**, 205422 (2014).

[14] N. Scheuschner, O. Ochedowski, A.-M. Kaulitz, R. Gillen, M. Schleberger, and J. Maultzsch, Phys. Rev. B **89**, 125406 (2014).

[15] C. Yim, M. O'Brien, N. McEvoy, S. Winters, I. Mirza, J. G. Lunney, and G. S. Duesberg, Appl. Phys. Lett. **104**, 103114:1– 5, (2014).

[16] T. Cao, G. Wang, W. Han, H. Ye, C. Zhu, J. Shi, Q. Niu, P. Tan, E. Wang, B. Liu, and J. Feng, Nat. Commun. **3**, 887, (2012).

[17] K. F. Mak, K. He, J. Shan, and T. F. Heinz, Nat. Nanotechnol. **7**, 494– 498 (2012).

[18] G. Sallen, L. Bouet, X. Marie, G. Wang, C. R. Zhu, W. P. Han, Y. Lu, P. H. Tan, T. Amand, B. L. Liu, and B. Urbaszek, Phys. Rev. B **86**, 081301, (2012).

[19] H. Zeng, J. Dai, W. Yao, D. Xiao, and X. Cui, Nat. Nanotechnol. **7**, 490–493, (2012).

[20] D. Xiao, G.-B. Liu, W. Feng, X. Xu, and W. Yao, Phys. Rev. Lett. **108**, 196802 (2012).

[21] A. M. Jones, H. Yu, N. J. Ghimire, S. Wu, G. Aivazian, J. S. Ross, B. Zhao, J. Yan, D. G. Mandrus, D. Xiao, W. Yao, and X. Xu, Nat. Nanotechnol. **8**, 634–638, (2013).

[22] D. Lagarde, L. Bouet, X. Marie, C. R. Zhu, B. L. Liu, T. Amand, P. H. Tan, and B. Urbaszek, Phys. Rev. Lett. **112**, 047401, (2014).

[23] K. F. Mak, K. L. McGill, J. Park, and P. L. McEuen, Science **344**, 1489– 1492 (2014).

[24] G. Wang, L. Bouet, D. Lagarde, M. Vidal, A. Balocchi, T. Amand, X. Marie, and B. Urbaszek, Phys. Rev. B. **90**, 075413, (2014).

[25] X. Xu, W. Yao, D. Xiao, and T. F. Heinz, Nat. Phys. **10**, 343– 350, (2014).

[26] K. He, N. Kumar, L. Zhao, Z. Wang, K. F. Mak, H. Zhao, and J. Shan *Phys. Rev. Lett.* **113**, 026803, (2014).

[27] A. Chernikov, T. C. Berkelbach, H. M. Hill, A. Rigosi, Y. Li, O. B. Aslan, D. R. Reichman, M. S. Hybertsen, and T. F. Heinz, Phys. Rev. Lett. **113**, 076802 (2014).

[28] M. M. Ugeda, A. J. Bradley, S.-F. Shi, F. H. da Jornada, Y. Zhang, D. Y. Qiu, S.-K. Mo, Z. Hussain, Z.-X. Shen, and F. Wang et al, Nat. Mater. **13**, 1091– 1095 (2014).

[29] Z. Ye, T. Cao, K. O'Brien, H. Zhu, X. Yin, Y. Wang, S. G. Louie, and X. Zhang, Nature **513**, 214 (2014).

[30] G. Wang, X. Marie, I. Gerber, T. Amand, D. Lagarde, L. Bouet, M. Vidal, A. Balocchi, and B. Urbaszek, Phys. Rev. Lett. **114**, 097403, (2015).

[31] C. Zhang, A. Johnson, C. L. Hsu, L. J. Li, and C. K. Shih, Nano Lett. **14**, 2443 (2014).

[32] A. R. Klots, A. K. M. Newaz, B. Wang, D. Prasai, H. Krzyzanowska, D. Caudel, N. J. Ghimire, J. Yan, B. L. Ivanov, and K. A. Velizhanin et al., Sci. Rep. **4**, 6608 (2014).

[33] H. M. Hill, A. F. Rigosi, C. Roquelet, A. Chernikov, T. C. Berkelbach, D. R. Reichman, M. S. Hybertsen, L. E. Brus, and T. F. Heinz, Nano Lett. **15**, 2992 (2015).

[34] K. F. Mak, K. He, C. Lee, G. H. Lee, J. Hone, T. F. Heinz, and J. Shan, Nat. Mater. **12**, 207– 211, (2013).

[35] J. S. Ross, S. Wu, H. Yu, N. J. Ghimire, A. M. Jones, G. Aivazian, J. Yan, D. G. Mandrus, D. Xiao, W. Yao, and X. Xu, Nat. Commun. **4**, 1474, (2013).

[36] W. Jin, P.-C. Yeh, N. Zaki, D. Chenet, G. Arefe, Y. Hao, A. Sala, T. O. Mentes, J. I. Dadap, A. Locatelli, J. Hone, R. M. Osgood Jr., Phys. Rev. B. **92,** 201409, (2015).

[37] D. Jariwala, V. K. Sangwan, L. J. Lauhon, T. J. Marks, and M. C. Hersam, ACS Nano **8**, 1102– 1120 (2014).

[38] K. Roy, M. Padmanabhan, S. Goswami, T. P. Sai, G. Ramalingam, S. Raghavan, and A. Ghosh, Nat. Nanotechnol. **8**, 826– 830, (2013).

[39] W. J. Yu, Z. Li, H. Zhou, Y. Chen, Y. Wang, Y. Huang, and X. Duan, Nat. Mater. **12**, 246– 252, (2012).

[40] M.-H. Chiu, C. Zhang, H. W. Shiu, C.-P. Chu, C.-H. Chen, C.-Y. S. Chang, C.-H. Chen, and M.-Y.Chou, et al, Nat. Commun. **6**, 7666 (2015).

[41] Y. Yu, S. Hu, L. Su, L. Huang, Y. Liu, Z. Jin, A. A. Purezky, D. B. Geohegan, K. W. Kim, and Y. Zhang, Nano Lett. **15**, 486, (2015).

[42] X. Hong, J. Kim, S. F. Shi, Y. Zhang, C. Jin, Y. Sun, S. Tongay, J. Wu, Y. Zhang, F. Wang, Nat. Nanotechnol. **9**, 682– 686, (2014).

[43] P. Rivera, J. R. Schaibley, A. M. Jones, J. S. Ross, S. Wu, G. Aivazian, P. Klement, N. J. Ghimire, J. Yan, and D. G. Mandrus, Nat. Commun. **6**, 6242, (2015).

[44] H. Fang, C. Battaglia, C. Carraro, S. Nemsak, B. Ozdol, J. S. Kang, H. A. Bechtel, S. B. Desai, F. Kronast, A. A. Unal, A. A, et al. Proc. Natl. Acad. Sci. U. S. A. **111**, 6198, (2014).

[45] Y. Gong, J. Lin, X. Wang, G. Shi, S. Lei, Z. Lin, X. Zou, G. Ye, R. Vajtai, B. Yakobson, H. Terrones, M. Terrones, B. K. Tay, J. Lou, S. T. Pantelides, Z. Liu, W. Zhou, and P. M. Ajayan, Nat. Mater. **13**, 1135-1142, (2014).

[46] M.-H. Chiu, M.-Y. Li, W. Zhang, W.-T. Hsu, W.-H. Chang, M. Terrones, H. Terrones, and L.-J. Li, ACS Nano **8**, 9649– 9656, (2014).

[47] K. Liu, Q. Yan, M. Chen, W. Fan, Y. Sun, J. Suh, D. Fu, S. Lee, J. Zhou, S. Tongay, J. Ji, J. B. Neaton, and J. Wu, Nano Lett. **14**, 5097–5103, (2014).

[48] S. Tongay, W. Fan, J. Kang, J. Park, U. Koldemir, J. Suh, D. S. Narang, K. Liu, J. Ji, J. Li, R. Sinclair, and J. Wu, Nano Lett. **14**, 3185– 3190, (2014).

[49] G. W. Shim, K. Yoo, S. B. Seo, J. Shin, D. Y. Jung, I. S. Kang, C. W. Ahn, B. J. Cho, and S. Y. Choi, ACS Nano **8**, 6655–6662, (2014).

[50] F. Ceballos, M. Z. Bellus, H. Chiu, and H. Zhao, ACS Nano **8**, 12717, (2014).

[51] A. F. Rigosi, H. M. Hill, Y. Li, A. Chernikov, and T. F. Heinz, Nano Lett. **15**, 5033, (2015).

[52] F. Ceballos, M.-G. Ju, S. D. Lane, X. C. Zeng, H. Zhao, Nano Lett. **17**, 1623, (2017).

[53] O. A. Ajayi, J. V. Ardelean, G. D. Shepard, J. Wang, A. Antony, T. Taniguchi, K. Watanabe, T. F. Heinz, S. Strauf, X.-Y. Zhu, and J. C. Hone, *arXiv:1702.05857*.

[54] C Lan, C. Li, S. Wang, T. He, Z. Zhou, D. Wei, H. Guo, H. Yang, and Y. Liu, J. Mater. Chem. C **5**, 1494-1500, (2017).

[55] J. He, N. Kumar, M. Z. Bellus, H.-Y. Chiu, D. He, Y. Wang, and H. Zhao, Nat. Commun. **5**, 5622, (2014).

[56] T. Georgiou, R. Jalil, B. D. Belle, L. Britnell, R. V. Gorbachev, S. V. Morozov, Y.-J. Kim, A. Gholinia, S. J. Haigh, O. Makarovsky, et al. Nat. Nanotechnol. **8**, 100-103, (2013).

[57] F. H. L. Koppens, T. Mueller, P. Avouris, A. C. Ferrari, M. S. Vitiello, and M. Polini, Nat. Nanotechnol. **9**, 780-793, (2014).

[58] A. Raja, A. Chaves, J. Yu, G. Arefe, H. M. Hill, A. F. Rigosi, T. C. Berkelbach, P. Nagler, C. Schuller, T. Korn, C. Nuckolls, J. Hone, L. E. Brus, T. F. Heinz, D. R. Reichman, and A. Chernikov, Nat Commun. **8,** 15251, (2017).

[59] J. He, D. He, Y. Wang, and H. Zhao, Opt. Express **25**, 1949-1957, (2017).

[60] See Supplemental Material at [URL will be inserted by publisher] for more information about the observed broadening, exciton peak redshifts, PL quenching, Raman spectroscopy of graphene, spatial and processing variation, and interface quality.

[61] H. Zhu, J. Wang, Z. Gong, Y. D. Kim, M. Gustafsson, J. Hone, and X. Zhu, *arXiv:1702.06366*.

[62] T. Korn, S. Heydrich, M. Hirmer, J. Schmutzler, and C. Schüller, Appl. Phys. Lett. **99**, 102109, (2011).

[63] M. Selig, G. Berghäuser, A. Raja, P. Nagler, C. Schüller, T. F. Heinz, T. Korn, A. Chernikov, E. Malic, and A. Knorr, Nat. Commun. **7**, 13279, (2016).

[64] A. Chernikov, A. M. van der Zande, H. M. Hill, A. F. Rigosi, A. Velauthapillai, J. Hone, and T. F. Heinz, Phys. Rev. Lett. **115**, 126802, (2015).

[65] W. Jin, P.-C. Yeh, N. Zaki, D. Zhang, J. T. Sadowski, A. Al-Mahboob, A. M. van Der Zande, D. A. Chenet, J. I. Dadap, I. P. Herman, P. Sutter, J. Hone, and R. M. Osgood Jr Phys. Rev. Lett. **111,** 106801, (2013).

[66] S. Ulstrup, J. Katoch, R. J. Koch, D. Schwarz, S. Singh, K. M. McCreary, H. K. Yoo, J. Xu, B. T. Jonker, R. K. Kawakami, A. Bostwick, E. Rotenberg, and C. Jozwiak, ACS Nano **10**, 10058–10067, (2016).

[67] S. Ulstrup, A. G. Čabo, J. A. Miwa, J. M. Riley, S. S. Grønborg, J. C. Johannsen, C. Cacho, O. Alexander, R. T. Chapman, E. Springate, M. Bianchi, M. Dendzik, J. V. Lauritsen, P. D. C. King, and P. Hofmann, ACS Nano **10**, 6315-6322, (2016).

[68] N. R. Wilson, P. V. Nguyen, K. Seyler, P. Rivera, A. J. Marsden, Z. P. L. Laker, G. C. Constantinescu, V. Kandyba, A. Barinov, N. D. M. Hine, X. Xu, and D. H. Cobden, Sci. Adv. **3**, 1601832, (2017).

[69] A. Raja, A. Montoya-Castillo, J. Zultak, X.-X. Zhang, Z. Ye, C. Roquelet, D. A. Chenet, A. M. van der Zande, P. Huang, S. Jockusch, J. Hone, D. R. Reichman, L. E. Brus, and T. F. Heinz, Nano Lett. **16**, 2328-2333, (2016).

[70] Z. Chen, S. Berciaud, C. Nuckolls, T. F. Heinz, and L. E. Brus, ACS Nano **4,** 2964-2968, (2010).

[71] F. Prins, A. J. Goodman, and W. A. Tisdale, Nano Lett. **14**, 6087–6091, (2014).

[72] F.: Federspiel, G. Froehlicher, M. Nasilowski, S. Pedetti, A. Mahmood, B. Doudin, S. Park, J.-O. Lee, D. Halley, B. Dubertret, P. Gilliot, and S. Berciaud, Nano Lett. **15**, 1252–1258, (2015).

[73] P. L. Hernández-Martínez, A. O. Govorov, and H. V. Demir, J. Phys. Chem. C **118**, 4951–4958, (2014).

[74] L. Gaudreau, K. J. Tielrooij, G. E. D. K. Prawiroatmodjo, J. Osmond, F. J. G. de Abajo, and F. H. L. Koppens, Nano Lett. **13**, 2030–2035, (2013).

[75] A. Naeem, F. Masia, S. Christodoulou, I. Moreels, P. Borri, and W. Langbein, Phys. Rev. B. **91**, 121302, (2015).

[76] W. Wurth and D. Menzel, Chem. Phys. **251**, 141, (2000).

[77] J. Gudde and U. Hofer, Prog. Surf. Sci. **80**, 49–91, (2005).

[78] A. Berkdemir, H. R. Gutiérrez, A. R. Botello-Méndez, N. Perea López, A. L. Elías, C.-I. Chia, B. Wang, V. H. Crespi, F. López-Urías, J.-C. Charlier, Sci. Rep. **3**, 1755, (2013).

[79] D. Sun, Y. Rao, G. A. Reider, G. Chen, Y. You, L. Brezin, A. R. Harutyunyan, and T. F. Heinz, Nano Lett. **14**, 5625, (2014).

[80] L. Wang, Z. Chen, C. Dean, T. Tanigushi, K. Watanabe, L. E. Brus, and J. Hone, *ACS Nano*, 2012, 6, 9314-9319.

[81] A. C. Ferrari, J. C. Meyer, V. Scardaci, C. Casiraghi, M. Lazzeri, F. Mauri, S. Piscanec, D. Jiang, K. S. Novoselov, S. Roth, and A. K. Geim, Phys. Rev. Lett. **97**, 187401, (2006).

[82] J. Yan, Y. Zhang, P. Kim, and A. Pinczuk, Phys, Rev. Lett. **98**, 166802, (2007).

[83] M. Bruna, A. K. Ott, M. Ijäs, D. Yoon, U. Sassi, and A. C. Ferrari, ACS Nano **8**, 7432-7441, (2014).

[84] A. Das, S. Pisana, B. Chakraborty, S. Piscanec, S. K. Saha, U. V. Waghmare, K. S. Novoselov, H. R. Krishnamurthy, A. K. Geim, A. C. Ferrari, A. K. Sood, Nat. Nanotechnol. **3**, 210–215, (2008).

TABLE OF CONTENTS GRAPHIC (END OF DOC)